

Article

CuFe₂O₄ Magnetic Nanoparticles as Heterogeneous Catalysts for Synthesis of Dihydropyrimidinones as Inhibitors of SARS-CoV-2 Surface Proteins—Insights from Molecular Docking Studies

Sónia A. C. Carabineiro ¹, Gullapalli B. Dharma Rao ², Lakhwinder Singh ³, Bendi Anjaneyulu ^{3,*} and Mozhgan Afshari ^{4,*}

¹ LAQV-REQUIMTE, Department of Chemistry, NOVA School of Science and Technology, Universidade NOVA de Lisboa, 2829-516 Caparica, Portugal; sonia.carabineiro@fct.unl.pt

² Department of Chemistry, Kommuri Pratap Reddy Institute of Technology, Hyderabad 500088, Telangana, India

³ Department of Chemistry, Faculty of Science, SGT University, Gurugram 122505, Haryana, India

⁴ Department of Chemistry, Shoushtar Branch, Islamic Azad University, Shoushtar, Iran

* Correspondence: anjaneyulu.bendi@gmail.com (B.A.); mozhgan.afshari@iau.ac.ir (M.A.)

Abstract: In this study, we present the highly efficient and rapid synthesis of substituted dihydropyrimidinone derivatives through an ultrasound-accelerated approach. We utilize copper ferrite (CuFe₂O₄) magnetic nanoparticles as heterogeneous catalysts, employing the well-known Biginelli reaction, under solvent-free conditions. The impact of the solvent, catalyst amount, and catalyst type on the reaction performance is thoroughly investigated. Our method offers several notable advantages, including facile catalyst separation, catalyst reusability for up to three cycles with the minimal loss of activity, a straightforward procedure, mild reaction conditions, and impressive yields, ranging from 79% to 95%, within short reaction times of 20 to 40 min. Furthermore, in the context of fighting COVID-19, we explore the potential of substituted dihydropyrimidinone derivatives as inhibitors of three crucial SARS-CoV-2 proteins. These proteins, glycoproteins, and proteases play pivotal roles in the entry, replication, and spread of the virus. Peptides and antiviral drugs targeting these proteins hold great promise in the development of effective treatments. Through theoretical molecular docking studies, we compare the binding properties of the synthesized dihydropyrimidinone derivatives with the widely used hydroxychloroquine molecule as a reference. Our findings reveal that some of the tested molecules exhibit superior binding characteristics compared to hydroxychloroquine, while others demonstrate comparable results. These results highlight the potential of our synthesized derivatives as effective inhibitors in the fight against SARS-CoV-2.

Keywords: COVID-19; heterocycles; multicomponent reaction; Biginelli reaction; dihydropyrimidinones; heterogeneous catalyst; copper ferrite; nanoparticles; molecular docking; hydroxychloroquine



Citation: Carabineiro, S.A.C.; Dharma Rao, G.B.; Singh, L.; Anjaneyulu, B.; Afshari, M. CuFe₂O₄ Magnetic Nanoparticles as Heterogeneous Catalysts for Synthesis of Dihydropyrimidinones as Inhibitors of SARS-CoV-2 Surface Proteins—Insights from Molecular Docking Studies. *Processes* **2023**, *11*, 2294. <https://doi.org/10.3390/pr11082294>

Academic Editor: Fabio Carniato

Received: 5 July 2023

Revised: 25 July 2023

Accepted: 26 July 2023

Published: 31 July 2023



Copyright: © 2023 by the authors. Licensee MDPI, Basel, Switzerland. This article is an open access article distributed under the terms and conditions of the Creative Commons Attribution (CC BY) license (<https://creativecommons.org/licenses/by/4.0/>).

1. Introduction

The Biginelli reaction, a well-known and highly significant multicomponent reaction (MCR), has been a cornerstone in organic chemistry since its establishment by the Italian chemist Pietro Biginelli in 1891 [1,2]. This reaction enables the synthesis of dihydropyrimidinone (DHPM) derivatives, belonging to an important class of N-heterocyclic compounds. The reaction proceeds via the one-pot condensation of an aliphatic or aryl aldehyde, β-ketoester, and urea or thiourea under strong acidic conditions [1]. DHPMs and their diverse derivatives have been garnering enormous amounts of attention due to their wide range of biological activities over the past few decades [3,4]. These compounds exhibit remarkable potential as anticancer, antiviral, antimalarial, anti-inflammatory, anti-tubercular, antidiabetic, antiepileptic, antileishmanial, antibacterial, and antiproliferative

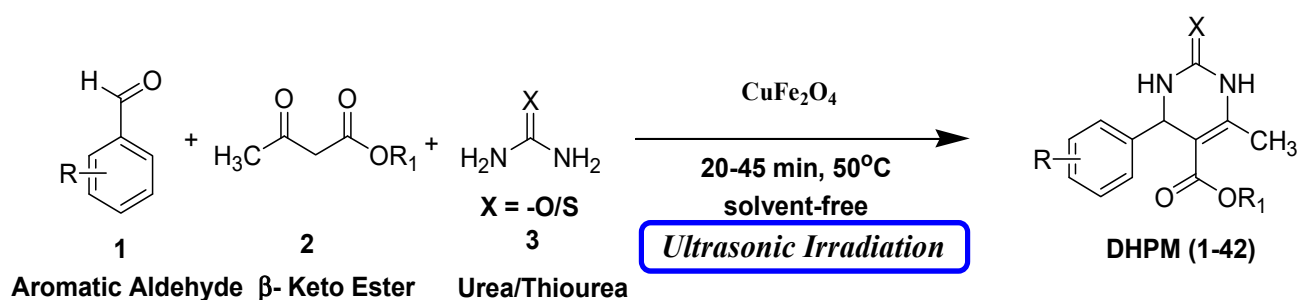
agents. Moreover, several multifunctionalized DHPMs demonstrated their efficacy as A2B receptor antagonists, powerful calcium channel blockers, mPGES-1 inhibitors, α -adrenergic antagonists, and antihypertensive drugs [4–10]. The diverse pharmacological properties exhibited by these Biginelli MCR-derived compounds make them a subject of continuous interest for researchers and pharmaceutical chemists.

Numerous researchers recognized the importance of the Biginelli reaction and explored various catalysts as alternatives to traditional protic acids like HCl [1], concentrated H₂SO₄, and silica H₂SO₄ [11]. These catalysts include Lewis acids, solid acids, ionic liquids, and bio- and organocatalysts [12,13]. The introduction of these catalysts has enabled significant improvements in reaction efficiency, selectivity, and environmentally friendly characteristics. By circumventing the drawbacks associated with traditional catalysts, these innovative approaches offer promising solutions to long-standing challenges in the Biginelli reaction. One notable advantage of these catalysts is their heterogeneous nature, which facilitates catalyst recovery and recycling, thus mitigating the need for complex separation techniques.

Nanoparticles with large surface areas show remarkable catalytic activity in organic reactions, and the utilization of heterogeneous catalysts for the Biginelli reaction has already been explored [14–16]. In recent decades, ultrasound-mediated processes gained significant traction, with reports of several successful chemical procedures employing this technique [17–20]. Ultrasound-assisted reactions offer numerous advantages over conventional heating methods, including faster reaction times, the reduced formation of undesirable by-products, the production of clean products with high yields, the simplicity of operation in open systems, and milder reaction conditions. These favorable attributes make ultrasound technology inherently “green”, “clean”, and “eco-friendly”. However, the application of ultrasound in heterocyclic ring formation has been relatively underutilized [21,22]. Motivated by this research gap and our fascination with ultrasound-assisted heterocyclic synthesis [23], we elaborated an effective and fast method for the synthesis of substituted 3,4-dihydropyrimidin-2-(1H)-ones, as reported in this study.

In the 21st century, nanotechnology gained significant focus and recognition as a key area of research and development across various scientific and technological fields. Magnetic nanoparticles (MNPs), owing to their facile synthesis, easy separation, reusability, high recoverability, technological significance, and diverse biological applications, garnered significant attention [24]. One of the most notable types of iron-based magnetic materials are ferrite nanoparticles, which exhibit superior structural and chemical stability compared to bulk ferrites [25,26]. Among metal ferrite nanoparticles, copper ferrite (CuFe₂O₄) is a particularly interesting choice for the synthesis of various heterocycles [27,28]. Compared to traditional catalytic systems, CuFe₂O₄ nanoparticles offer several advantages such as an easy setup, recyclability, cleaner reaction profiles, and the reduced generation of organic waste. Surprisingly, despite these beneficial properties, CuFe₂O₄ nanoparticles have not yet been explored in the synthesis of 3,4-dihydropyrimidin-2-(1H)-ones under ultrasonic conditions.

However, the existing methods for the Biginelli reaction using alternative catalysts still face various challenges, including prolonged reaction times, harsh reaction conditions, difficulties in product isolation, by-product formation, and lower yields. Consequently, there is a pressing need to develop novel catalysts that overcome these limitations. Building upon our ongoing efforts to synthesize a diverse range of biologically active compounds [29–32], we sought to create a library of DHPM derivatives. Here, we present a straightforward, efficient, and environmentally friendly procedure for the synthesis of 3,4-dihydropyrimidin-2-(1H)-ones (DHPMs). This approach involves the combination of β -ketoester, urea/thiourea, and aromatic aldehyde in the presence of a small amount of CuFe₂O₄ magnetic nanoparticles as innovative and eco-friendly heterogeneous catalysts. Remarkably, this reaction proceeds under a temperature of 50 °C and solvent-free conditions with the aid of ultrasonic treatment (Scheme 1).



Scheme 1. Biginelli reaction using CuFe₂O₄ nanoparticles under solvent-free ultrasonic irradiation (UI).

The emergence of the SARS-CoV-2 virus, responsible for the devastating COVID-19 outbreak, has led to the widespread occurrence of severe acute respiratory syndrome, posing a critical global public health emergency. Given its unprecedented impact, it is imperative to devise an efficacious therapeutic strategy to effectively control and manage infections. Existing medications show limited efficacy in individuals with comorbidities and immunological deficiencies. Consequently, researchers have been diligently working toward the development of novel and effective anti-infection drugs [33–35]. Glycoproteins and proteases play indispensable roles in viral entry, replication, and spread, making them prime targets for antiviral drugs. Peptides, with their high specificity, effectiveness, and safety [36–38], hold a special place in therapeutic approaches.

In recent years, numerous studies employing ligand and structure-based computational methodologies have risen to the challenge of identifying potential COVID-19 antiviral agents through virtual screening methods. Moreover, a notable advancement in this pursuit involves the development of heterocyclic substances that primarily target the COVID-19 main protease. Among these, nitrogen-containing heterocycles have emerged as particularly promising antivirals against coronaviruses, demonstrating their efficacy through the specific targeting of the primary protease of the virus (the main protease). The ability of these nitrogenous heterocycles to establish essential hydrogen bonds with specific biological targets makes them valuable candidates for drug development [39].

Molecular docking emerged as a highly valuable approach in the quest for new drugs targeting specific proteins. Among the various forms of docking, protein–ligand docking holds particular importance in the pharmaceutical industry. It enables the exploration of correct ligand conformations within a protein structure, being a powerful tool for drug discovery [29,40,41]. In line with this, we conducted molecular docking studies of 13 synthesized compounds with three key proteins associated with COVID-19: the main protease (PDB: 6LU7) [41], the pre-fusion spike glycoprotein with a single receptor-binding domain (PDB: 6VSB) [42], and the papain-like protease of SARS-CoV-2 (PDB: 6W9C) [43]. Autodock Vina and Discovery Studio Visualizer [44] software were employed for these docking studies.

2. Results and Discussion

2.1. Characterization of CuFe₂O₄ Nanoparticles

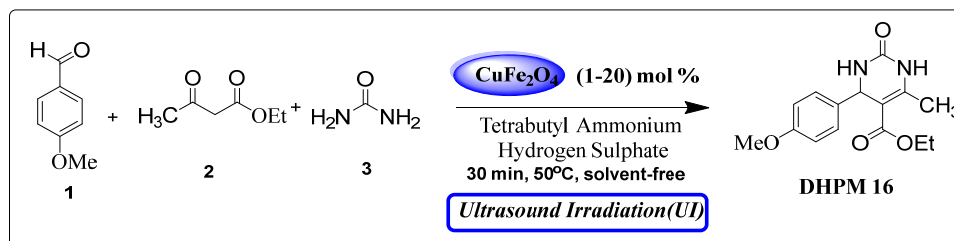
CuFe₂O₄ nanoparticles were successfully synthesized via a straightforward co-precipitation process employing NaOH as the precipitating reagent. The nanoparticles were characterized via X-ray diffraction (XRD), Fourier-transform infrared spectroscopy (FT-IR), and transmission electron microscopy (TEM) [45,46].

2.2. 3,4-Dihydropyrimidin-2(1H)-one Synthesis

To assess the effectiveness of the proposed synthetic procedure, a model reaction was conducted at 50 °C using 4-methoxybenzaldehyde (1), ethyl acetoacetate (2) and urea (3). The reaction was performed in different solvents using an ultrasound irradiation approach (with an operating frequency of 24 kHz), with CuFe₂O₄ nanoparticles as the catalytic component and a minimal amount of tetrabutyl ammonium hydrogen sulfate

(TBAHS) serving as the phase transfer catalyst (Table 1). The selection of solvents plays a crucial role in multi-component reactions (MCRs) due to the presence of various reactive functional groups.

Table 1. Optimization of reaction conditions ^a.



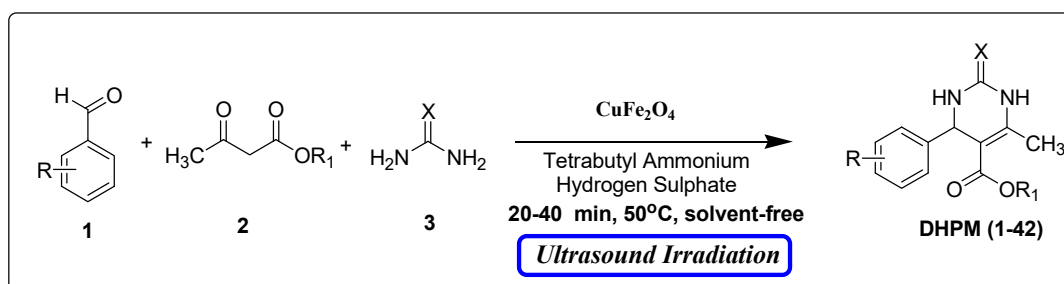
Entry	CuFe ₂ O ₄ mol%	Time (min.)	Yield % ^b
1	-	30	36
2	1	30	48
3	3	30	62
4	5	30	78
5	10	30	92
6	20	30	92

^a Reaction conditions: **1** (1.0 mmol), **2** (1.0 mmol), **3** (1.2 mmol), CuFe₂O₄ (1–20) mol%, 50 °C, UI (30 min).
^b Isolated Yield.

Observations revealed that the desired product was obtained in yields of 57% in H₂O, 49% in toluene, 63% in CHCl₃, 72% in CH₃CN with an extended reaction time, and 85% in EtOH. Notably, utilizing 10 mol% CuFe₂O₄ catalysts yielded ethyl 4-(4-methoxyphenyl)-6-methyl-2-oxo-1,2,3,4-tetrahydropyrimidine-5-carboxy (DHPM16) with a maximum yield of 92% under solvent-free conditions (Table 2, entry 16).

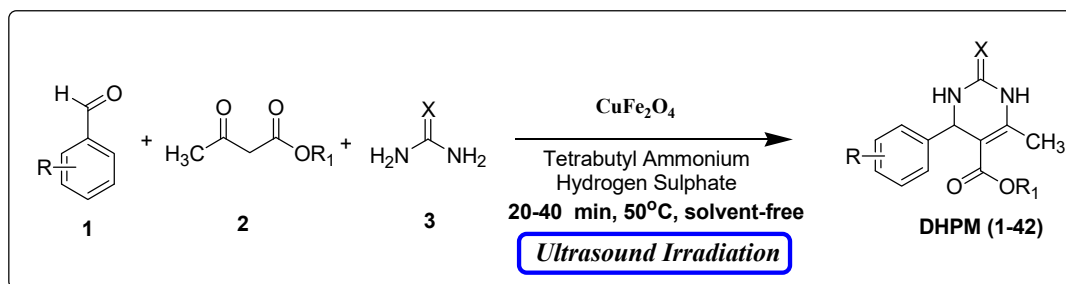
However, increasing the catalyst concentration from 10% to 20% did not lead to an improvement in the yield of compound DHPM16, as indicated in Table 1. Furthermore, several aryl aldehydes and β-keto esters were tested in combination with urea/thiourea to explore the reaction, and the results are presented in Table 2. The results showed the condensation was completed within 20–40 min and products were obtained in high yields (79–95%).

The model reaction (Table 2, entry 16) was conducted using various catalysts with a reaction time of 30 min. The yields obtained were 81%, 84%, 85%, 89%, and 92% when ZnO nanoparticles, TiO₂ nanoparticles, CaFe₂O₄ nanoparticles, CoFe₂O₄/Cu(OH)₂ nanocomposites, and CuFe₂O₄ nanoparticles were used, respectively (Table 3). In contrast, conducting the reaction without a catalyst resulted in a significantly lower yield of 65%. Additionally, the efficiency of copper ferrite for the synthesis of the model compound 3,4-dihydropyrimidin-2(1H)-one was also compared with some of the materials reported in the earlier literature, as shown in Table 3. From the collected data, it is clear that our catalytic conditions, in terms of the absence of solvent, cost-effective process, time, and high yield, are efficient in the fast synthesis of the products.

Table 2. CuFe₂O₄ magnetic nanoparticles employed in the synthesis of 3,4-dihydropyrimidinones via Biginelli condensation ^a.

S. No	R	R ₁	X	Time (min)	Product	Yield (%) ^b	Observed M. P	Reported M. P Ref.
1	4-Me-		O	40	DHPM1	94	154–156	148–150 [47]
2	4-OMe-		O	30	DHPM2	95	158–160	152–154 [47]
3	4-OEt-		O	40	DHPM3	95	132–134	128–130 [47]
4	4-OMe-		O	35	DHPM4	92	178–180	180–182 [47]
5	4-NO ₂ -		O	40	DHPM5	92	170–172	174–176 [47]
6	4-Cl-		O	25	DHPM6	91	160–162	156–158 [47]
7	3-Cl-		O	30	DHPM7	94	192–194	194–196 [47]
8	4-OMe-		O	20	DHPM8	90	168–170	168–170 [47]
9	4-OMe-		O	40	DHPM9	92	160–162	158–160 [47]
10	4-OMe-		O	25	DHPM10	88	160–162	158–160 [42]
11	3-Cl-		O	30	DHPM11	90	202–204	-
12	4-OMe-		O	30	DHPM12	92	198–200	200–202 [47]
13	4-OMe-		O	40	DHPM13	94	180–182	178–180 [47]

Table 2. Cont.



S. No	R	R ₁	X	Time (min)	Product	Yield (%) ^b	Observed M. P	Reported M. P Ref.
14	4-H-	OEt	O	20	DHPM14	94	200–202	198–200 [48]
15	4-Cl-	OEt	O	30	DHPM15	90	210–212	211–213 [48]
16	4-OMe-	OEt	O	30	DHPM16	92	206–208	200–202 [48]
17	4-Me-	OEt	O	40	DHPM17	89	202–204	205–206 [48]
18	2-Cl-	OEt	O	25	DHPM18	81	214–216	211–214 [48]
19	4-OH-	OEt	O	25	DHPM19	79	208–210	209–220 [48]
20	3-NO ₂ -	OEt	O	30	DHPM20	86	218–220	217 [48]
21	4-Br-	OEt	O	30	DHPM21	88	198–200	197 [48]
22	4-NO ₂ -	OEt	O	35	DHPM22	90	244–246	243–245 [48]
23	2,4-di-Cl-	OEt	O	25	DHPM23	80	202–204	202–204 [48]
24	3-OH-	OEt	S	30	DHPM24	81	180–182	183–184 [48]
25	4-H-	OEt	S	40	DHPM25	91	204–204	200–205 [48]
26	3-NO ₂ -	OEt	S	35	DHPM2	87	208–210	206–207 [48]
27	3,4-di-OMe-	OEt	O	30	DHPM27	80	176–178	175–177 [48]
28	3,4-di-OMe-	OEt	S	20	DHPM28	72	212–214	212–214 [48]
29	3,4,5-tri-OMe	OEt	O	20	DHPM29	68	180–182	180–181 [48]
30	4-Me-	OEt	S	35	DHPM30	84	194–196	194–196 [48]
31	3-Br-	OEt	O	30	DHPM31	88	190–192	190–192 [48]
32	4-Br-	OEt	S	25	DHPM32	80	180–182	182–183 [48]
33	4-OH-	OMe	O	20	DHPM33	85	244–246	242–244 [48]
34	4-OMe-	OMe	S	25	DHPM34	80	152–154	152–154 [48]
35	4-NO ₂ -	OMe	O	30	DHPM35	84	230–232	233–235 [48]
36	4-F-	OMe	O	30	DHPM36	89	194–196	193–195 [48]
37	4-H-	OMe	O	35	DHPM37	92	206–208	208–210 [48]
38	4-Br-	OMe	S	25	DHPM38	84	152–154	153–154 [48]
39	4-OH-	OMe	S	20	DHPM39	79	246–248	245–246 [48]
40	4-Cl-	OMe	O	20	DHPM40	89	204–206	204–206 [48]
41	4-OMe-	OMe	O	40	DHPM41	90	190–192	189–193 [48]
42	4-Br-	OMe	O	40	DHPM42	91	220–222	218–220 [48]

^a Reaction conditions: 1 (1.0 mmol), 2 (1.0 mmol), 3 (1.2 mmol), CuFe_2O_4 (1–20 mol%), 50 °C, UI (40 min)

^b Isolated Yield.

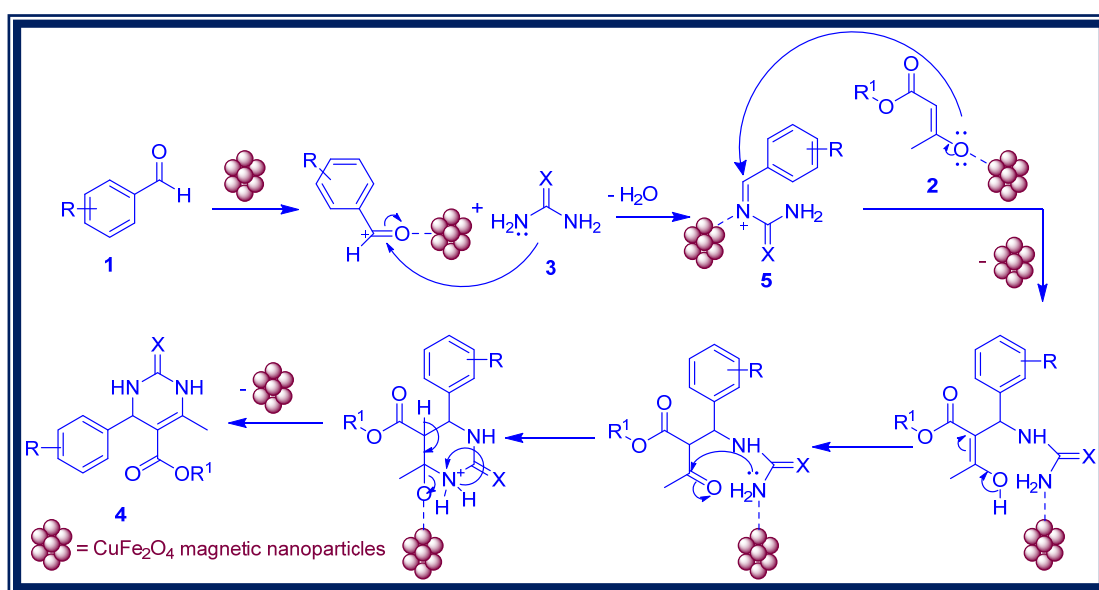
Table 3. Comparative performance of CuFe_2O_4 magnetic nanoparticles with other catalysts in the preparation of 3,4-dihydropyrimidin-2(1H)-one (DHPM16).

Entry	Catalyst	Condition	Time (min)	Yield ^a	Reference
1	CoFe_2O_4	Solvent-free/80 °C	90	85.4	[49]
2	HoCl_3	Solvent-free/80 °C/UI	150	92	[50]
3	n- TiO_2 - NH_2	Solvent-free/100 °C	270	91	[51]
4	$\text{Y}(\text{OAc})_3 \cdot \text{X H}_2\text{O}$	Acetic acid/reflux	270	89	[52]
5	ZnO	Solvent-free/TBAHS/50 °C/UI	30	81	This work
6	TiO_2	Solvent-free/TBAHS/50 °C/UI	30	84	This work
7	CaFe_2O_4	Solvent-free/TBAHS/50 °C/UI	30	85	This work
8	$\text{CoFe}_2\text{O}_4/\text{Cu}(\text{OH})_2$	Solvent-free/TBAHS/50 °C/UI	30	89	This work
9	CuFe_2O_4	Solvent-free/TBAHS/50 °C/UI	30	92	This work
10	-	Solvent-free/TBAHS/50 °C/UI	30	65	This work

^a Isolated Yield (%).

To assess the sustainability and reusability of CuFe_2O_4 nanoparticles, a recovery and reusability study was conducted. The nanoparticles were subjected to a reaction involving 4-methoxybenzaldehyde (1, R = -4 - OMe), ethyl acetoacetate (2, $\text{R}_1 = -\text{OEt}$), and urea (3, X = -O) in the presence of CuFe_2O_4 (10 mol%) under ultrasound irradiation, at 50 °C, for 20 min. The results showed the reusability of the catalyst up to three cycles, reducing the activity from 92 to 80%. The slight decrease in activity can be attributed to the inevitable loss of catalyst during the recycling process.

A proposed mechanism for the formation of 3,4-dihydropyrimidin-2(1H)-ones is depicted in Scheme 2 [53]. The overall catalytic activity of a chemical reaction is primarily dependent on the availability of acidic sites on the catalyst surface. In the synthesis of dihydropyrimidinones, Lewis and Bronsted acid catalysts are typically employed. With tripositive Fe^{3+} and dipositive Cu^{2+} ions present, CuFe_2O_4 nanoparticles exhibit strong Lewis acid characteristics. Thus, the acidic sites of the CuFe_2O_4 catalyst play a crucial role in regulating the entire catalytic cycle during the synthesis of dihydropyrimidinones.

**Scheme 2.** Proposed mechanism for the synthesis of 3,4-dihydropyrimidinone derivatives via Biginelli reaction using CuFe_2O_4 magnetic nanoparticles.

The Lewis acidity of Fe^{3+} arises from its higher electronegativity, while the acidity of Cu^{2+} results from the acquisition of a stable and filled d-subshell upon electron acceptance. Initially, the Lewis acidic sites of the catalyst interact with the oxygen lone pairs on the carbonyl group of aromatic aldehydes, creating a positive charge at the carbonyl carbon. Subsequently, these sites react with urea, leading to the formation of intermediate 5 through water molecule elimination. The cyclization of the formed intermediate with β -ketoester then yields the corresponding 3,4-dihydropyrimidin-2-(1H)-ones (Scheme 2).

2.3. Molecular Docking Studies

Based on a comprehensive literature review [37–40,54], proteins that play a crucial role in the pathogenesis of SARS-CoV-2 were selected as molecular targets. The crystal structures of the COVID-19 main protease (PDB: 6LU7) at a resolution of 2.16 Å, pre-fusion spike glycoprotein with a single receptor-binding domain (PDB: 6VSB) at a resolution of 3.46 Å, and the papain-like protease of SARS-CoV-2 (PDB: 6W9C) at a resolution of 2.7 Å were obtained from the Protein Data Bank and analyzed.

The results obtained from the molecular docking studies of 13 potential ligands with different proteins of SARS-CoV-2 are summarized in Table 4. The interactions between ligands and proteins were analyzed using various models of ligand–protein interactions, and their binding affinities (docking scores) were determined. The docking scores provided an indication of the binding strength between the ligands and the target proteins.

To further investigate the ligand properties, DFT (Density Functional Theory) studies were conducted. These studies provided additional insights into the electronic and structural properties of the ligands.

The docked models with the lowest binding energy and highest binding affinity were identified as the most stable ligand–target protein complexes. Ligands with the highest binding affinities were selected for further analysis. The structures with high docking scores were visually inspected to identify specific amino acids involved in ligand–protein binding, providing valuable information about the binding interactions at the molecular level.

Table 4. Results of molecular docking studies.

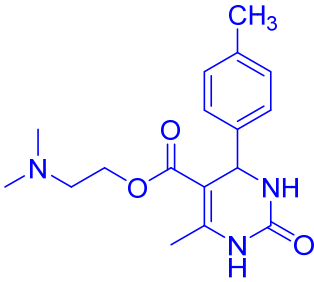
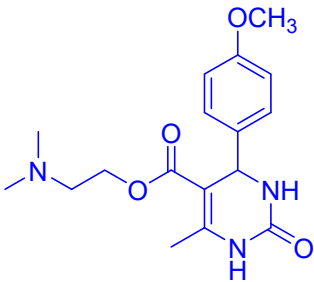
Ligand	Ligand Structure	Optimized Geometry Energy (au) (DFT Studies)	Binding Affinity (kcal/mol)		
			For SARS-CoV-2 Main Protease (6LU7)	For S-Glyco-Protein (6VSB)	For Papain-like Protease (6W9C)
DHPM1		−1111.12	−6.4	−5.2	−4.7
DHPM2		−1031.25	−6.0	−4.5	−4.9

Table 4. Cont.

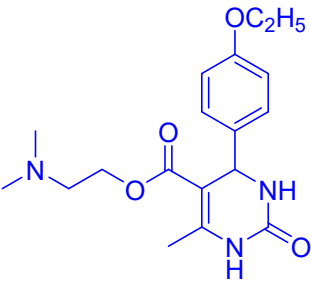
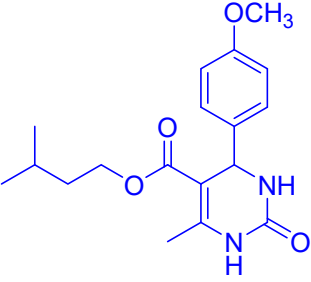
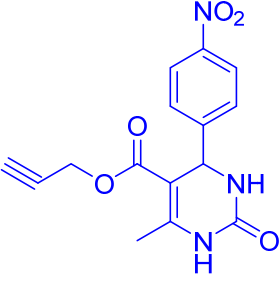
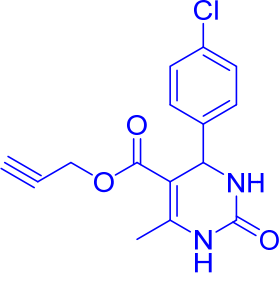
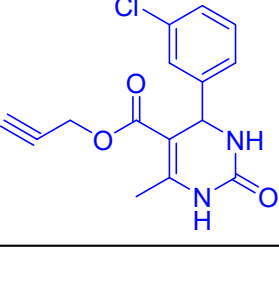
Ligand	Ligand Structure	Optimized Geometry Energy (au) (DFT Studies)	Binding Affinity (kcal/mol)		
			For SARS-CoV-2 Main Protease (6LU7)	For S-Glyco-Protein (6VSB)	For Papain-like Protease (6WNC)
DHPM3		−1109.89	−6.2	−4.6	−4.8
DHPM4		−1119.98	−6.1	−4.7	−4.3
DHPM5		−1375.04	−6.4	−5.0	−5.0
DHPM6		−1375.04	−6.4	−4.7	−4.6
DHPM7		−1029.97	−6.3	−4.7	−4.5

Table 4. Cont.

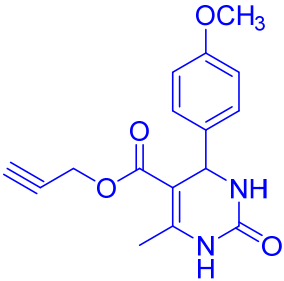
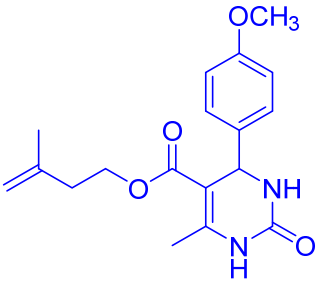
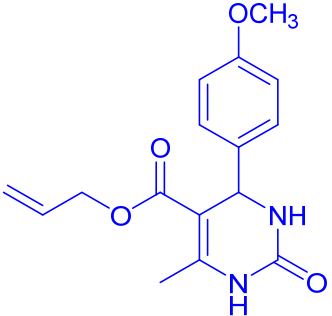
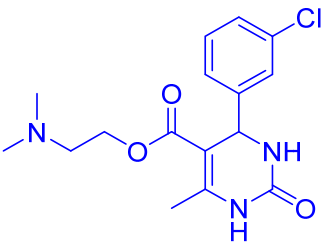
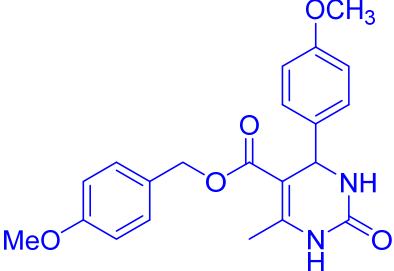
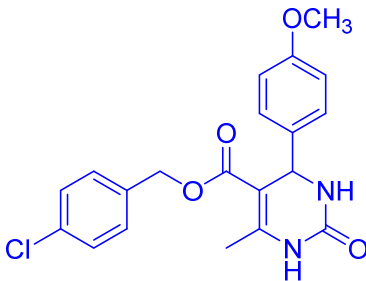
Ligand	Ligand Structure	Optimized Geometry Energy (au) (DFT Studies)	Binding Affinity (kcal/mol)		
			For SARS-CoV-2 Main Protease (6LU7)	For S-Glyco-Protein (6VSB)	For Papain-like Protease (6WNC)
DHPM8		−1051.91	−6.0	−4.8	−4.5
DHPM9		−1127.14	−6.2	−4.6	−4.3
DHPM10		−1166.47	−6.1	−4.7	−4.3
DHPM11		−1472.21	−6.3	−4.6	−4.6
DHPM12		−1299.48	−7.3	−5.2	−4.6

Table 4. Cont.

Ligand	Ligand Structure	Optimized Geometry Energy (au) (DFT Studies)	Binding Affinity (kcal/mol)		
			For SARS-CoV-2 Main Protease (6LU7)	For S-Glyco-Protein (6VSB)	For Papain-like Protease (6WNC)
DHPM13		−1644.55	−7.1	−5.0	−4.5
Reference	Hydroxychloroquine	-	−6.5	−6.0	−6.3

The data obtained from the molecular docking studies were compared with hydroxychloroquine [32], which served as a reference molecule. Several of the synthesized compounds demonstrated favorable interactions, forming two or more electrostatic bonds with the target proteins. Docking results of 13 different ligands with pre-fusion spike glycoprotein and papain-like protease of SARS-CoV-2 are presented in Supplementary Information.

As an example of ligand–enzyme interactions, the binding interactions of DHPM 12 (Figure 1) and DHPM 13 (Figure 2) with the SARS-2 main protease (PDB: 6LU7) are illustrated.

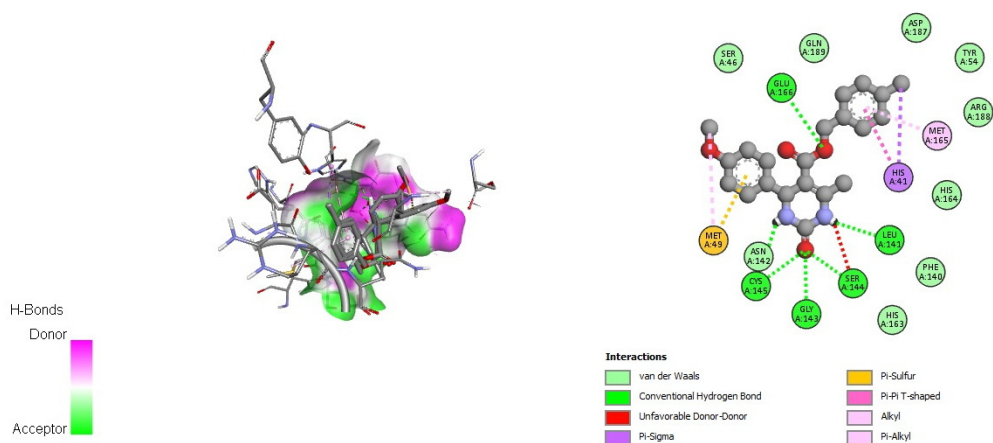


Figure 1. Docking interactions of DHPM 12 with SARS-CoV-2 main protease (PDB: 6LU7).

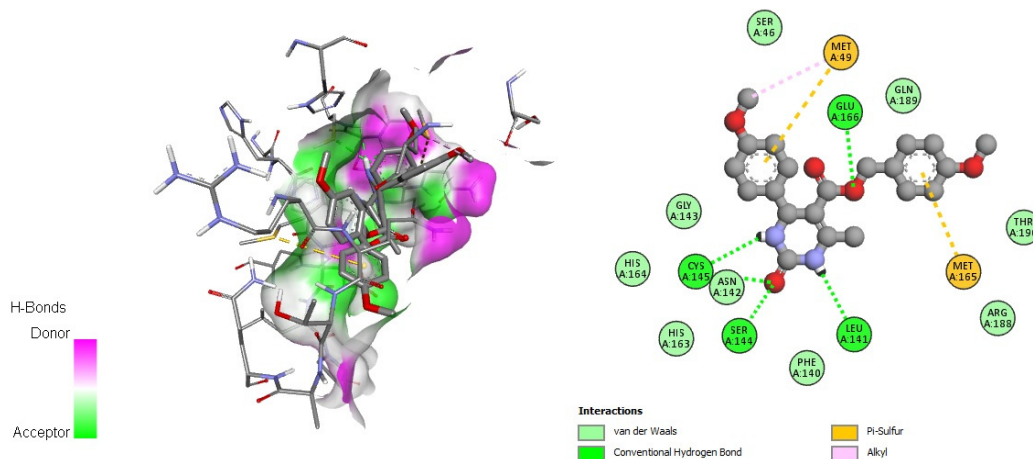


Figure 2. Docking interactions of DHPM 13 with SARS-CoV-2 main protease (PDB: 6LU7).

Figures 3 and 4 show the interactions of the ligands DHPM 1 and DHPM 12 with the pre-fusion spike glycoprotein (PDB: 6VSB).

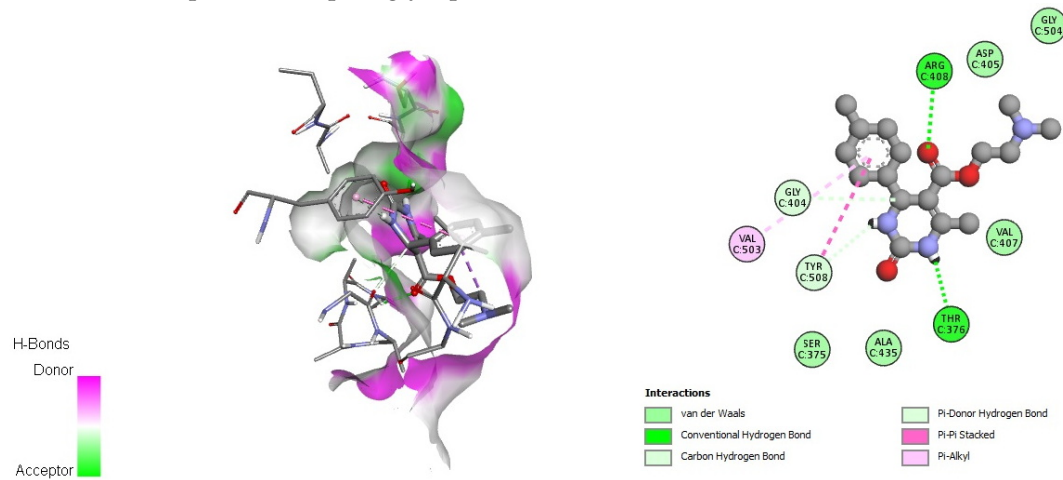


Figure 3. Docking interactions of DHPM 1 with pre-fusion spike glycoprotein (PDB: 6VSB).

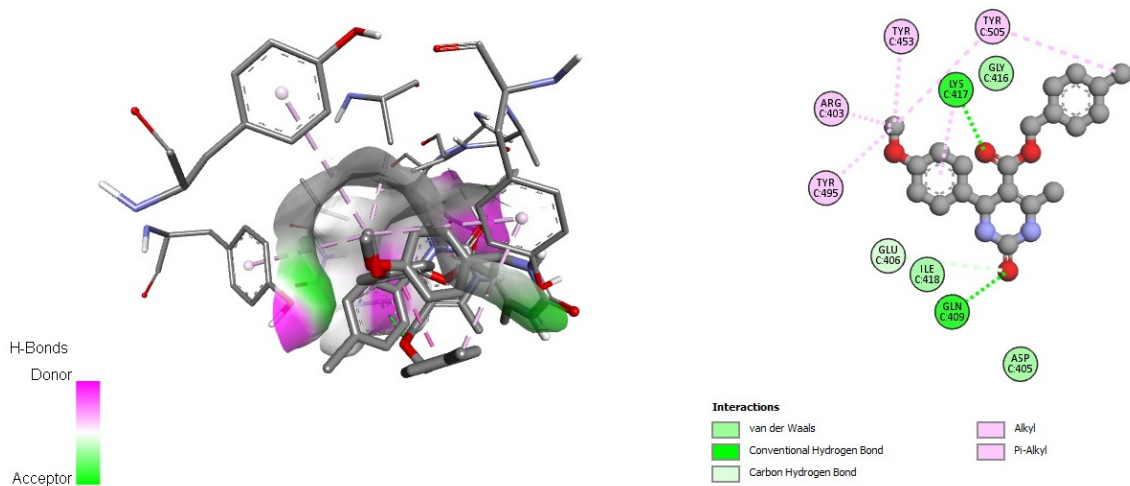


Figure 4. Docking interactions of DHPM 12 with pre-fusion spike glycoprotein (PDB: 6VSB).

Figures 5 and 6 display the interactions between the ligands DHPM 2 and DHPM 5 and the papain-like protease of SARS-CoV-2 (PDB: 6W9C).

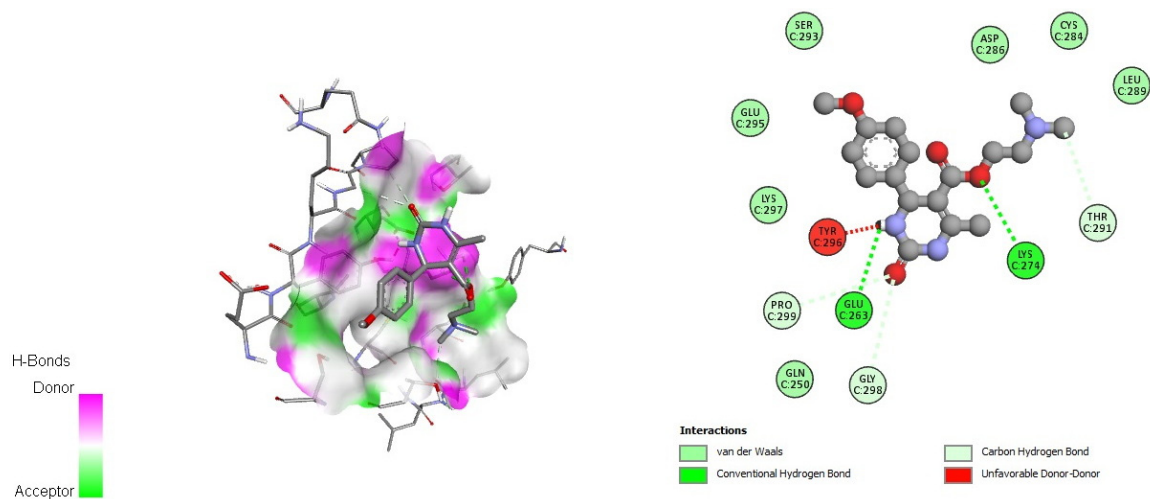


Figure 5. Docking interactions of DHPM 2 with papain-like protease of SARS-CoV-2 (PDB: 6W9C).

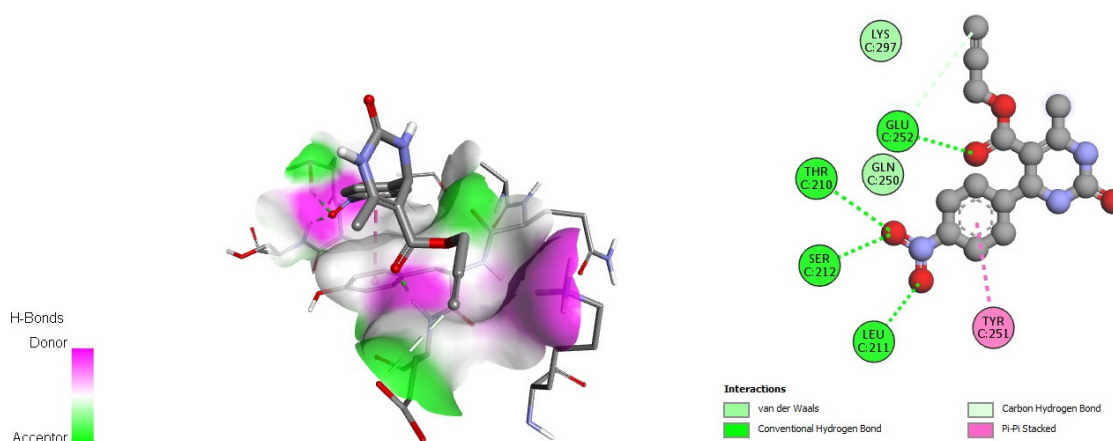


Figure 6. Docking interactions of DHPM 5 with papain-like protease of SARS-CoV-2 (PDB: 6W9C).

3. Experimental Details

3.1. Synthesis of Copper Ferrite Nanoparticles

$\text{Cu}(\text{NO}_3)_2 \cdot 5\text{H}_2\text{O}$ (0.5M) and $\text{Fe}(\text{NO}_3)_3 \cdot 9\text{H}_2\text{O}$ (1.0M) were separately dissolved in distilled water and thoroughly mixed at 70 °C. The solution pH was adjusted to 12 via the drop-wise addition of 6 M NaOH solution using a burette. Once the desired pH was reached, no more NaOH was added, and the mixture was further stirred for a designated period. The formed precipitate was subjected to agitation for 2.5 h at 70 °C. Subsequently, the precipitate was filtered, followed by washing with ethanol and deionized water until a pH of 7 was obtained. The washed precipitate was then dried at 60 °C. The resulting powder was further subjected to calcination at 300 °C for 2.5 h, resulting in the formation of CuFe_2O_4 nanoparticles [46].

3.2. Synthesis of 3,4-Dihydropyrimidinones via Ultrasonic Irradiation Method

To a mixture of aromatic aldehydes 1 (1 mmol), β -keto ester 2 (1 mmol), urea/thiourea 3 (1.2 mmol), a minimal amount (0.005 mmol) of tetrabutyl ammonium hydrogen sulfate (TBAHS), and CuFe_2O_4 nanoparticles (10 mol percent) were added, followed by stirring. The reaction mixture was then subjected to sonication (TOMY, UD 201, acoustic power 45 W with digital water bath temperature controller) at 50 °C for the specified duration, as mentioned in Table 2. The reaction progress was followed with TLC (ethyl acetate/n-hexane (10:3)). Once the reaction was completed, the mixture was cooled to room temperature and washed with brine. Ethyl acetate was used for the extraction process. The catalyst was separated from the extraction mixture using a magnetic separation method.

The organic layer was separated and dried with anhydrous sodium sulfate. The solution was then concentrated under low pressure. To purify the crude product, recrystallization was carried out from a mixture of hot ethanol and water, resulting in the formation of 3,4-dihydropyrimidinone derivatives with high yields. Structural confirmation of the majority of the products was performed using physical techniques. Additionally, spectroscopic data such as $^1\text{H-NMR}$ and $^{13}\text{C-NMR}$ were employed to confirm the structures of some products, with a comparison to data in the literature. $^1\text{H NMR}$ spectra of some compounds are presented in Supplementary Information.

3.3. Analytical Data of Some Representative Compounds

*Ethyl*4-(4-methoxyphenyl)-6-methyl-2-oxo-1,2,3,4-tetrahydropyrimidine-5-carboxylate (DHPM16): M. P: 206–208 °C; IR (KBr): 3520, 3275, 2899, 1665, 762, 702 cm^{-1} ; $^1\text{H NMR}$ (400 MHz, $\text{DMSO-}d_6$): 1.04–1.10 (t, 3H, $-\text{OCH}_2\text{CH}_3$), 2.22 (s, 3H, $-\text{CH}_3$), 3.70 (s, 3H, $-\text{OCH}_3$), 3.91–3.96 (q, 2H, $-\text{OCH}_2\text{CH}_3$), 5.05 (s, 1H, $-\text{CH-Ar}$), 6.82–6.87 (d, 2H, $J = 8.0$ Hz, Ar-H), 7.11–7.09 (d, 2H, $J = 8.0$ Hz, Ar-H), 7.62 (s, 1H, NH); 9.11 (s, 1H, NH); $^{13}\text{C NMR}$: (100 MHz, $\text{DMSO-}d_6$) 14.2, 17.6, 53.2, 55.8, 61.7, 106.4, 114.1, 125.7, 135.6, 147.3, 150.2, 156.5, 158.6, 167.2; ESI-MS:

m/z 291.18 $[M+1]^+$, *Anal.* Calcd for $C_{15}H_{18}N_2O_4$: C, 62.06; H, 6.25; N, 9.65. Found: C, 62.10; H, 6.24; N, 9.68.

Ethyl 4-(4-hydroxyphenyl)-6-methyl-2-oxo-1,2,3,4-tetrahydropyrimidine-5-carboxylate (DHPM19): M. P: 209–220 °C; IR (KBr): 3518, 3235, 2985, 1648, 762, 686 cm^{-1} ; 1H NMR (400 MHz, DMSO- d_6): 1.07–1.04 (t, 3H, $-OCH_2CH_3$), 2.18 (s, 3H, $-CH_3$), 3.97–3.90 (q, 2H, $-OCH_2CH_3$), 4.99 (s, 1H, $-CH-Ar$), 6.65–6.63 (d, 2H, $J = 8.0$ Hz, Ar-H), 6.99–6.97 (d, 2H, $J = 8.0$ Hz, Ar-H), 7.57 (s, 1H, NH); 9.07 (s, 1H, NH); 9.28 (s, 1H, OH); ^{13}C NMR: (100 MHz, DMSO- d_6) 14.8, 17.4, 53.2, 61.7, 106.4, 115.7, 126.4, 135.9, 147.6, 150.2, 156.5, 167.2; ESI-MS: m/z 277.11 $[M+1]^+$, *Anal.* Calcd for $C_{14}H_{16}N_2O_4$: C, 60.86; H, 5.84; N, 10.14. Found: C, 60.84; H, 5.86; N, 10.12.

Methyl 4-(4-fluorophenyl)-6-methyl-2-oxo-1,2,3,4-tetrahydropyrimidine-5-carboxylate (DHPM36): M. P: 194–196 °C; IR (KBr): 3526, 3238, 2965, 1668, 790, 676 cm^{-1} ; 1H NMR (400 MHz, DMSO- d_6) δ 9.23 (s, 1H, NH), 7.74 (s, 1H, NH), 7.29–7.17 (m, 2H, Ar-H), 7.11 (t, $J = 8.7$ Hz, 2H, Ar-H), 5.12 (s, 1H, $-CH-Ar$), 3.50 (s, 3H, $-OCH_3$), 2.22 (s, 3H, $-CH_3$). ^{13}C NMR (101 MHz, DMSO) δ 166.23, 163.01, 160.60, 160.08, 152.51, 149.27, 141.41, 141.38, 128.68, 128.60, 115.74, 115.53, 99.39, 53.65, 51.27, 18.30. ESI-MS: m/z 265.07 $[M+1]^+$, *Anal.* Calcd for $C_{13}H_{13}FN_2O_3$: C, 59.09; H, 4.96; N, 10.60, O, 18.16. Found: C, 59.11; H, 5.02; N, 10.57, O, 18.20.

3.4. Molecular Docking and DFT Studies

The crystal structures of the COVID-19 proteins were obtained from the Protein Data Bank and analyzed using Discovery Studio Visualizer. Molecular docking studies were performed using the software Autodock Vina 4.2 and Discovery Studio Visualizer [44]. To further investigate the ligand properties, DFT (Density Functional Theory) studies were conducted using Spartan 14 software with the B3LYP method and the 6-311++G (d, p) basis set [46]. The structures with high docking scores were visually inspected using Discovery Studio 4.0 software.

4. Conclusions

We successfully developed an efficient and trouble-free ultrasound-accelerated method for synthesizing 3,4-dihydropyrimidinone compounds using copper ferrite as a catalyst. Notably, this technique adheres to the principles of green chemistry as it operates without the use of solvents, demonstrating operational simplicity, economic viability, and environmental friendliness. The method proves to be both time- and cost-effective, allowing for the high-yielding production of compounds with swift reaction times. Moreover, its versatility enables its application for various purposes.

In addition to the synthetic achievements, we conducted molecular docking studies on 13 selected compounds out of the total 42 compounds. The results revealed that the compounds DHPM-12 and DHPM 13 exhibit enhanced interaction with the binding site of COVID-19 major protease (Mpro) compared to the reference ligand hydroxychloroquine. Similarly, the interactions of DHPM 1 and DHPM 12 with pre-fusion spike glycoprotein (PDB: 6VSB) and DHPM 2 and DHPM 5 with the papain-like protease of SARS-CoV-2 (PDB: 6W9C) correlate well with the interactions of the reference ligand, hydroxychloroquine. These findings provide valuable insights into the potential of these compounds as effective inhibitors.

This communication serves as a pathway for young researchers to delve into experimental investigations of the interactions between different 3,4-dihydropyrimidinone derivatives and various COVID-19 viruses.

Supplementary Materials: The following supporting information can be downloaded at: <https://www.mdpi.com/article/10.3390/pr11082294/s1>. Molecular Docking Studies; Docking results of 13 different ligands with COVID-19 main protease at 2.16 Å resolution (PDB: 6LU7); Docking results of 13 different ligands with Pre-fusion spike glycoprotein with single receptor binding domain at 3.46 Å resolution (PDB: 6VSB); Docking results of 13 different ligands with papain-like protease of SARS-CoV-2 at 2.7 Å resolution (PDB: 6W9C); Spectral data (1H NMR) of some representative compounds.

Author Contributions: Conceptualization, G.B.D.R.; Methodology, G.B.D.R.; Formal analysis, G.B.D.R. and B.A.; Investigation, S.A.C.C., G.B.D.R., B.A. and M.A.; Data curation, G.B.D.R.; Writing—original draft, L.S.; Writing—review & editing, S.A.C.C., L.S., B.A. and M.A.; Supervision, M.A.; Funding acquisition, S.A.C.C. All authors have read and agreed to the published version of the manuscript.

Funding: S.A.C.C. is grateful to Fundação para a Ciência e a Tecnologia (FCT), Portugal for Scientific Employment Stimulus-Institutional Call (CEEC-INST/00102/2018) and to the Associate Laboratory for Green Chemistry-LAQV financed by national funds from FCT/MCTES (UIDB/50006/2020 and UIDP/5006/2020).

Data Availability Statement: Data will be made available upon request.

Acknowledgments: Anjaneyulu Bendi and Lakhwinder Singh express special gratitude to the management of SGT University, Gurugram, and G.B. Dharma Rao conveys his sincere thanks to the management of KPRIT, Hyderabad, for providing the facilities to conduct the research and submit this article for publication. All the authors are grateful to JNU, New Delhi, for XRD, FT-IR, and VSM characterizations and IARI, New Delhi, for TEM characterization. The authors also wish to acknowledge the support of this work by the Research Council of Shoushtar Branch, Islamic Azad University, Shoushtar, Iran. S.A.C.C. is grateful to Fundação para a Ciência e a Tecnologia (FCT), Portugal for Scientific Employment Stimulus-Institutional Call (CEEC-INST/00102/2018) and to the Associate Laboratory for Green Chemistry-LAQV financed by national funds from FCT/MCTES (UIDB/50006/2020 and UIDP/5006/2020).

Conflicts of Interest: The authors declare that they have no conflict of interest regarding the content presented in this article.

References

1. Biginelli, P.; Gazz, P. Synthesis of 3, 4-dihydropyrimidin-2 (1H)-ones. *Gazz. Chim. Ital.* **1893**, *23*, 360–416.
2. Tron, G.C.; Minassi, A.; Appendino, G. *Pietro Biginelli: The Man behind the Reaction*; Wiley Online Library: Hoboken, NJ, USA, 2011.
3. Matos, L.H.S.; Masson, F.T.; Simeoni, L.A.; Homem-de-Mello, M. Biological activity of dihydropyrimidinone (DHPM) derivatives: A systematic review. *Eur. J. Med. Chem.* **2018**, *143*, 1779–1789. [[CrossRef](#)] [[PubMed](#)]
4. Kappe, C.O. Biologically active dihydropyrimidones of the Biginelli-type—A literature survey. *Eur. J. Med. Chem.* **2000**, *35*, 1043–1052. [[CrossRef](#)] [[PubMed](#)]
5. Franklin, A.S.; Ly, S.K.; Mackin, G.H.; Overman, L.E.; Shaka, A. Application of the tethered Biginelli reaction for enantioselective synthesis of batzelladine alkaloids. Absolute configuration of the tricyclic guanidine portion of batzelladine B. *J. Org. Chem.* **1999**, *64*, 1512–1519. [[CrossRef](#)] [[PubMed](#)]
6. Atwal, K.S.; Swanson, B.N.; Unger, S.E.; Floyd, D.M.; Moreland, S.; Hedberg, A.; O'Reilly, B.C. Dihydropyrimidine calcium channel blockers. 3. 3-Carbamoyl-4-aryl-1, 2, 3, 4-tetrahydro-6-methyl-5-pyrimidinecarboxylic acid esters as orally effective antihypertensive agents. *J. Med. Chem.* **1991**, *34*, 806–811. [[CrossRef](#)] [[PubMed](#)]
7. Grover, G.J.; Dzwonczyk, S.; McMullen, D.M.; Normandin, D.E.; Parham, C.S.; Slep, P.G.; Moreland, S. Pharmacologic profile of the dihydropyrimidine calcium channel blockers SQ 32,547 and SQ 32,946. *J. Cardiovasc. Pharmacol.* **1995**, *26*, 289–294. [[CrossRef](#)]
8. Rovnyak, G.C.; Kimball, S.D.; Beyer, B.; Cucinotta, G.; DiMarco, J.D.; Gougoutas, J.; Hedberg, A.; Malley, M.; McCarthy, J.P. Calcium entry blockers and activators: Conformational and structural determinants of dihydropyrimidine calcium channel modulators. *J. Med. Chem.* **1995**, *38*, 119–129. [[CrossRef](#)]
9. Hu, E.H.; Sidler, D.R.; Dolling, U.-H. Unprecedented catalytic three component one-pot condensation reaction: An efficient synthesis of 5-alkoxycarbonyl-4-aryl-3, 4-dihydropyrimidin-2 (1H)-ones. *J. Org. Chem.* **1998**, *63*, 3454–3457. [[CrossRef](#)]
10. Phukan, M.; Kalita, M.K.; Borah, R. A new protocol for Biginelli (or like) reaction under solvent-free grinding method using Fe (NO₃)₃·9 H₂O as catalyst. *Green Chem. Lett. Rev.* **2010**, *3*, 329–334. [[CrossRef](#)]
11. Salehi, P.; Dabiri, M.; Zolfigol, M.A.; Fard, M.A.B. Silica sulfuric acid: An efficient and reusable catalyst for the one-pot synthesis of 3, 4-dihydropyrimidin-2 (1H)-ones. *Tetrahedron Lett.* **2003**, *44*, 2889–2891. [[CrossRef](#)]
12. Oboudatian, H.S.; Naeimi, H.; Moradian, M. A Brønsted acidic ionic liquid anchored to magnetite nanoparticles as a novel recoverable heterogeneous catalyst for the Biginelli reaction. *RSC Adv.* **2021**, *11*, 7271–7279. [[CrossRef](#)] [[PubMed](#)]
13. Radai, Z.; Kiss, N.Z.; Keglevich, G. An overview of the applications of ionic liquids as catalysts and additives in organic chemical reactions. *Curr. Org. Chem.* **2018**, *22*, 533–556. [[CrossRef](#)]
14. Nazari, S.; Saadat, S.; Fard, P.K.; Gorjizadeh, M.; Nezhad, E.R.; Afshari, M. Imidazole functionalized magnetic Fe₃O₄ nanoparticles as a novel heterogeneous and efficient catalyst for synthesis of dihydropyrimidinones by Biginelli reaction. *Monatshfte Für Chem.-Chem. Mon.* **2013**, *144*, 1877–1882. [[CrossRef](#)]
15. Afshari, M.; Gorjizadeh, M.; Naseh, M. Supported sulfonic acid on magnetic nanoparticles used as a reusable catalyst for rapid synthesis of α -aminophosphonates. *Inorg. Nano-Met. Chem.* **2017**, *47*, 591–596. [[CrossRef](#)]

16. Afshari, M.; Carabineiro, S.A.; Gorjizadeh, M. Sulfonated Silica Coated CoFe₂O₄ Magnetic Nanoparticles for the Synthesis of 3, 4-Dihydropyrimidin-2 (1H)-One and Octahydroquinazoline Derivatives. *Catalysts* **2023**, *13*, 989. [[CrossRef](#)]
17. Marzag, H.; Robert, G.; Dufies, M.; Bougrin, K.; Auburger, P.; Benhida, R. FeCl₃-promoted and ultrasound-assisted synthesis of resveratrol O-derived glycoside analogs. *Ultrason. Sonochemistry* **2015**, *22*, 15–21. [[CrossRef](#)]
18. Vieira, M.M.; Dalberto, B.T.; Padilha, N.B.; Junior, H.C.; Rodembusch, F.S.; Schneider, P.H. Fast and efficient one-pot ultrasound-mediated synthesis of solid state (full color tunable) fluorescent indolizine derivatives. *Dye. Pigment.* **2023**, *216*, 111332. [[CrossRef](#)]
19. Ma, J.; Li, Y.; Wu, P.; Zhao, J.; Zheng, W. Ultrasound-Mediated Monodesulfonation of Polyphenol Sulfonate and One-Pot Generation of Alkyl Aryl Ether under Solvent-Free Conditions. *ChemistrySelect* **2023**, *8*, e202300659. [[CrossRef](#)]
20. Shabalala, N.G.; Kerru, N.; Maddila, S.; van Zyl, W.E.; Jonnalagadda, S.B. Ultrasound-mediated catalyst-free protocol for the synthesis of bis-3-methyl-1-phenyl-1H-pyrazol-5-ols in aqueous ethanol. *Chem. Data Collect.* **2020**, *28*, 100467. [[CrossRef](#)]
21. Chatel, G. How sonochemistry contributes to green chemistry? *Ultrason. Sonochemistry* **2018**, *40*, 117–122. [[CrossRef](#)]
22. Bendi, A.; Atri, S.; Rao, G.D.; Raza, M.J.; Sharma, N. Ultrasound-Accelerated, Concise, and Highly Efficient Synthesis of 2-Oxazoline Derivatives Using Heterogenous Calcium Ferrite Nanoparticles and Their DFT Studies. *J. Chem.* **2021**, *2021*, 7375058. [[CrossRef](#)]
23. Sharma, P.; Sharma, N.; Kashyap, G.; Bhagat, S. A concise and regioselective synthesis of 6-bromo-5-methoxy-1 H-indole-3-carboxylic acid and its derivatives: Strategic development toward core moiety of Herdmanine D. *Synth. Commun.* **2020**, *50*, 719–725. [[CrossRef](#)]
24. Eisavi, R.; Karimi, A. CoFe₂O₄/Cu(OH)₂ magnetic nanocomposite: An efficient and reusable heterogeneous catalyst for one-pot synthesis of β-hydroxy-1, 4-disubstituted-1, 2, 3-triazoles from epoxides. *RSC Adv.* **2019**, *9*, 29873–29887. [[CrossRef](#)] [[PubMed](#)]
25. Fernandes, R.J.; Magalhães, C.A.; Amorim, C.O.; Amaral, V.S.; Almeida, B.G.; Castanheira, E.M.; Coutinho, P.J. Magnetic nanoparticles of zinc/calcium ferrite decorated with silver for photodegradation of dyes. *Materials* **2019**, *12*, 3582. [[CrossRef](#)] [[PubMed](#)]
26. Kharisov, B.I.; Dias, H.R.; Kharissova, O.V. Mini-review: Ferrite nanoparticles in the catalysis. *Arab. J. Chem.* **2019**, *12*, 1234–1246. [[CrossRef](#)]
27. Peymanfar, R.; Azadi, F.; Yassi, Y. Preparation and characterization of CuFe₂O₄ nanoparticles by the sol-gel method and investigation of its microwave absorption properties at Ku-band frequency using silicone rubber. *Proceedings* **2018**, *2*, 1155.
28. Nikolić, V.N.; Vasić, M.M.; Kisić, D. Observation of c-CuFe₂O₄ nanoparticles of the same crystallite size in different nanocomposite materials: The influence of Fe³⁺ cations. *J. Solid State Chem.* **2019**, *275*, 187–196. [[CrossRef](#)]
29. Bendi, A.; Rao, G.B.D. Strategic One-pot Synthesis of Glycosyl Annulated Phosphorylated/Thiophosphorylated 1, 2, 3-Triazole Derivatives Using CuFe₂O₄ Nanoparticles as Heterogeneous Catalyst, their DFT and Molecular Docking Studies as Triazole Fungicides. *Lett. Org. Chem.* **2023**, *20*, 568–578. [[CrossRef](#)]
30. Rao, G.D.; Anjaneyulu, B.; Kaushik, M. Greener and expeditious one-pot synthesis of dihydropyrimidinone derivatives using non-commercial β-ketoesters via the Biginelli reaction. *RSC Adv.* **2014**, *4*, 43321–43325. [[CrossRef](#)]
31. Rao, G.D.; Anjaneyulu, B.; Kaushik, M. A facile one-pot five-component synthesis of glycoside annulated dihydropyrimidinone derivatives with 1, 2, 3-triazol linkage via transesterification/Biginelli/click reactions in aqueous medium. *Tetrahedron Lett.* **2014**, *55*, 19–22.
32. Anjaneyulu, B.; Rao, G.D.; Nagakalyan, S. Synthesis and DFT studies of 1, 2-disubstituted benzimidazoles using expeditious and magnetically recoverable CoFe₂O₄/Cu(OH)₂ nanocomposite under solvent-free condition. *J. Saudi Chem. Soc.* **2021**, *25*, 101394. [[CrossRef](#)]
33. Gangadaran, P.; Padinjarathil, H.; Rajendran, S.H.S.; Jogalekar, M.P.; Hong, C.M.; Aruchamy, B.; Rajendran, U.M.; Gurusagarajan, S.; Krishnan, A.; Ramani, P. COVID-19 and diabetes: What do we know so far? *Exp. Biol. Med.* **2022**, *247*, 1330–1334. [[CrossRef](#)] [[PubMed](#)]
34. Abdel-Latif, E.; Khatab, T.; Fekri, A.; Khalifa, M. Synthesis of New Binary Thiazole-Based Heterocycles and Their Molecular Docking Study as COVID-19 Main Protease (M pro) Inhibitors. *Russ. J. Gen. Chem.* **2021**, *91*, 1767–1773. [[CrossRef](#)]
35. Kim, J.; Zhang, J.; Cha, Y.; Koltz, S.; Funt, J.; Escalante Chong, R.; Barrett, S.; Kusko, R.; Zeskind, B.; Kaufman, H. Advanced bioinformatics rapidly identifies existing therapeutics for patients with coronavirus disease-2019 (COVID-19). *J. Transl. Med.* **2020**, *18*, 257. [[CrossRef](#)]
36. Krishnan, A.; Gangadaran, P.; Chavda, V.P.; Jogalekar, M.P.; Muthusamy, R.; Valu, D.; Vadivalagan, C.; Ramani, P.; Laishevcev, A.; Katari, N.K. Convalescent serum-derived exosomes: Attractive niche as COVID-19 diagnostic tool and vehicle for mRNA delivery. *Exp. Biol. Med.* **2022**, *247*, 1244–1252. [[CrossRef](#)] [[PubMed](#)]
37. Deshpande, R.R.; Tiwari, A.P.; Nyayanit, N.; Modak, M. In silico molecular docking analysis for repurposing therapeutics against multiple proteins from SARS-CoV-2. *Eur. J. Pharmacol.* **2020**, *886*, 173430. [[CrossRef](#)]
38. Hu, X.; Cai, X.; Song, X.; Li, C.; Zhao, J.; Luo, W.; Zhang, Q.; Ekumi, I.O.; He, Z. Possible SARS-coronavirus 2 inhibitor revealed by simulated molecular docking to viral main protease and host toll-like receptor. *Future Virol.* **2020**, *15*, 359–368. [[CrossRef](#)]
39. Musa, A.; Abulkhair, H.S.; Aljuhani, A.; Rezki, N.; Abdelgawad, M.A.; Shalaby, K.; El-Ghorab, A.H.; Aouad, M.R. Phenylpyrazolone-1,2,3-triazole Hybrids as Potent Antiviral Agents with Promising SARS-CoV-2 Main Protease Inhibition Potential. *Pharmaceuticals* **2023**, *16*, 463. [[CrossRef](#)]
40. Narkhede, R.R.; Cheke, R.S.; Ambhore, J.P.; Shinde, S.D. The molecular docking study of potential drug candidates showing anti-COVID-19 activity by exploring of therapeutic targets of SARS-CoV-2. *Eurasian J. Med. Oncol.* **2020**, *4*, 185–195.

41. Sayed, A.M.; Alhadrami, H.A.; El-Gendy, A.O.; Shamikh, Y.I.; Belbahri, L.; Hassan, H.M.; Abdelmohsen, U.R.; Rateb, M.E. Microbial natural products as potential inhibitors of SARS-CoV-2 main protease (Mpro). *Microorganisms* **2020**, *8*, 970. [[CrossRef](#)]
42. Wrapp, D.; Wang, N.; Corbett, K.S.; Goldsmith, J.A.; Hsieh, C.-L.; Abiona, O.; Graham, B.S.; McLellan, J.S. Cryo-EM structure of the 2019-nCoV spike in the prefusion conformation. *Science* **2020**, *367*, 1260–1263. [[CrossRef](#)] [[PubMed](#)]
43. Osipiuk, J.; Jedrzejczak, R.; Tesar, C.; Endres, M.; Stols, L.; Babnigg, G.; Kim, Y.; Michalska, K.; Joachimiak, A. The crystal structure of papain-like protease of SARS CoV-2. *RSCB PDB* **2020**, *10*. [[CrossRef](#)]
44. Morris, G.M.; Huey, R.; Lindstrom, W.; Sanner, M.F.; Belew, R.K.;Goodsell, D.S.; Olson, A.J. AutoDock4 and AutoDockTools4: Automated docking with selective receptor flexibility. *J. Comput. Chem.* **2009**, *30*, 2785–2791. [[CrossRef](#)] [[PubMed](#)]
45. Ali, K.; Bahadur, A.; Jabbar, A.; Iqbal, S.; Ahmad, I.; Bashir, M.I. Synthesis, structural, dielectric and magnetic properties of CuFe₂O₄/MnO₂ nanocomposites. *J. Magn. Magn. Mater.* **2017**, *434*, 30–36. [[CrossRef](#)]
46. Bendi, A.; Dharma Rao, G.B.; Sharma, N.; Tomar, R.; Singh, L. Solvent-Free Synthesis of Glycoside Annulated 1, 2, 3-Triazole Based Dihydropyrimidinones using Copper Ferrite Nanomaterials as Heterogeneous Catalyst and DFT Studies. *ChemistrySelect* **2022**, *7*, e202103910. [[CrossRef](#)]
47. Anjaneyulu, B.; Rao, G.D.; Bajaj, T. Click chemistry: In vitro evaluation of glycosyl hybrid phosphorylated/thiophosphorylated 1,2,3-triazole derivatives as irreversible acetyl cholinesterase (AChE) inhibitors. *Results Chem.* **2021**, *3*, 100093. [[CrossRef](#)]
48. Khabazzadeh, H.; Kermani, E.T.; Jazinizadeh, T. An efficient synthesis of 3, 4-dihydropyrimidin-2 (1H)-ones catalyzed by molten [Et₃NH][HSO₄]. *Arab. J. Chem.* **2012**, *5*, 485–488. [[CrossRef](#)]
49. Chandel, M.; Ghosh, B.K.; Moitra, D.; Patra, M.K.; Vadera, S.R.; Ghosh, N.N. Synthesis of various ferrite (MFe₂O₄) nanoparticles and their application as efficient and magnetically separable catalyst for biginelli reaction. *J. Nanosci. Nanotechnol.* **2018**, *18*, 2481–2492. [[CrossRef](#)]
50. Kakaei, S.; Sid Kalal, H.; Hoveidi, H. Ultrasound assisted one-pot synthesis of dihydropyrimidinones using holmium chloride as catalyst. *J. Sci. Islam. Repub. Iran* **2015**, *26*, 117–123.
51. Tabrizian, E.; Amoozadeh, A.; Shamsi, T. A novel class of heterogeneous catalysts based on toluene diisocyanate: The first amine-functionalized nano-titanium dioxide as a mild and highly recyclable solid nanocatalyst for the Biginelli reaction. *React. Kinet. Mech. Catal.* **2016**, *119*, 245–258. [[CrossRef](#)]
52. Aridoss, G.; Jeong, Y.-T. A convenient one-pot Biginelli reaction catalyzed by Y(OAc)₃: An improved protocol for the synthesis of 3, 4-dihydropyrimidin-2 (1H)-ones and their sulfur analogues. *Bull. Korean Chem. Soc.* **2010**, *31*, 863–868. [[CrossRef](#)]
53. Kumar, A.; Rout, L.; Achary, L.S.K.; Dhaka, R.S.; Dash, P. Greener route for synthesis of aryl and alkyl-14H-dibenzo [aj] xanthenes using graphene oxide-copper ferrite nanocomposite as a recyclable heterogeneous catalyst. *Sci. Rep.* **2017**, *7*, 42975. [[CrossRef](#)] [[PubMed](#)]
54. Owis, A.; El-Hawary, M.; El Amir, D.; Aly, O.; Abdelmohsen, U.; Kamel, M. Molecular docking reveals the potential of *Salvadora persica* flavonoids to inhibit COVID-19 virus main protease. *RSC Adv.* **2020**, *10*, 19570–19575. [[CrossRef](#)] [[PubMed](#)]

Disclaimer/Publisher's Note: The statements, opinions and data contained in all publications are solely those of the individual author(s) and contributor(s) and not of MDPI and/or the editor(s). MDPI and/or the editor(s) disclaim responsibility for any injury to people or property resulting from any ideas, methods, instructions or products referred to in the content.